DYNAMIC FORCE SENSORS AND THEIR APPLCIATIONS IN FLUIDIZED BEDS

Shyam Sundaram[1*], Allan Issangya[1] and S.B. Reddy Karri[1]

[1]*Particulate Solid Research, Inc*
4201 W 36th St, Bldg.A, Chicago, IL 60632
[*]Email : *shyam.sundaram@psri.org*

Abstract - The internals in fluidized bed processes, such as heat exchanger tubes, are subject to forces which are due to bubble dynamics and particle motion. Understanding the nature of these forces are industrially important since erosion and excessive vibrations of the internals can lead to process reliability issues. Preliminary tests were performed using a dynamic force sensor in PSRI's 2D fluidized bed unit (30-cm (12-in) wide by 2.54-cm (1-in) deep) with 760 μm size glass beads and 76 μm FCC equilibrium catalyst particles. The bed was at minimum fluidization and a single bubble was injected at different injection pressures. The sensor was mounted directly above a gas injection port used to inject a single bubble in the fluidized bed. Videos of the rising bubble and the response from the sensor were synchronized to quantify the forces from the bubble roof and wake. In the resulting waveform, the initial force caused by the injection of the bubble was the highest followed by lesser forces from wake and the roof. Tests were also conducted to quantify forces from gas jets, below and beyond the minimum fluidization velocity for the bed. There were two events that resulted in forces that were much larger than those observed from the rising bubbles. These random events, over a period, may be significant with respect to potential damage to fluidized bed internals.

1. INTRODUCTION

Fluidized beds may contain internals for the efficient mixing of bubbles and the emulsion phase, for the mitigation of gas bypassing, a phenomenon demonstrated by Karri et al. (2004) in deep beds of Group A materials and for temperature control with heating/cooling coils. T. H. Nguyen and J. R. Grace (1978) wrote that these internals can be subjected to random buffeting forces imparted by the rising bubbles or jets on the internals or tube bundles. The forces are dynamic in nature depending upon the residence time of the particles on tube bundles and the natural bubbling frequency of the bed (i.e., about 3-5 Hz). Since bubbles are primarily responsible for internals or tube vibrations and erosions, understanding bubble-internal interactions and origin of these forces are essential for the commercial reliability of these types of fluidized bed processes. Nagahashi et.al (1998) have measured forces acting on immersed tubes in fluidized beds. PSRI quantified these forces, using a dynamic force sensor which had the following characteristics:

- Can sense the rate of change of momentum when the bubbles come in contact with the tube bundle
- Has a very high response time
- Constant sensitivity over wide range of temperatures and pressures

2. SENSOR

The schematic drawing of the piezoelectric force sensor is shown in Fig. 1. The crystal is mounted on a dielectric base to minimize the leakage of charges. Attached to the crystal is a horizontal shaft to which a pressure-sensing diaphragm is connected. Whenever the diaphragm senses a change in pressure, the crystal is compressed and generates an electric potential, which is perpendicular to the direction of force. The output signal is then amplified and fed into a data acquisition system where the data is recorded in real time. The response time of the sensor is high (~ 2μs), which enables it to sense changes over orders of magnitude.

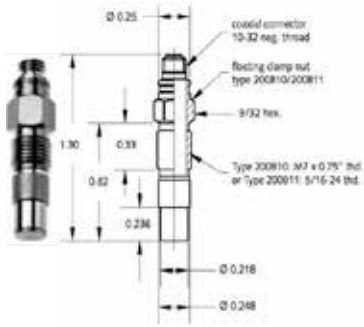

Fig. 1. Schematic of the piezoelectric force sensor

3. SIMPLIFIED CIRCUIT

The sensor has a high DC output impedance and can be modeled as a proportional voltage source and filter network. The voltage, V_0, at the source is directly proportional to the applied force, pressure, or strain. The output signal is then related to this mechanical force as if it had passed through the equivalent circuit. Fig. 2 shows the equivalent circuit response of the piezoelectric sensor. The inductance, L_m, is due to the seismic mass and inertia of the sensor itself. The series capacitance, Ce, is inversely proportional to the mechanical elasticity of the sensor. The parallel capacitance, Co, represents the static capacitance of the transducer. The parallel resistance, Ri, is the insulation leakage resistance of the transducer element. If the sensor is connected to a load resistance, this acts in parallel with the insulation resistance, both of which increase the high-pass cutoff frequency. The circuit can be simplified to an RC circuit with a time constant given by the product of resistance and capacitance. The voltage source, V, represents the voltage that develops due to excess surface charge on the crystal. The overall capacitance characteristic, Cs, represents the effective capacitance between the metallic plates. The load resistance, R1, results from the act of measuring the voltage across the terminals. The voltage developed across metallic plates is given by Q/Cs where Q is the charge. The discharge time constant, given by R1*Cs, is defined as the time required for the output voltage of the sensor to discharge to 37% of its original value in response to a zero-rise time step input function. It determines the low frequency response of the sensor and can be selected to give the required dynamic frequency range. Using a large time constant allows for measuring lower vibration frequencies, but at the cost of sensitivity. The higher the value of R1, the longer it will take for the charges to dissipate. The rate at which the charges discharge determines the sensor's ability to measure static loads. Thus, the quasi static measurements are more accurate for sensors that have larger discharge time constants. Fig. 3 shows the sensor's response to a constant load/force. The sensor responds instantly when a load is applied and the signal strength decreases exponentially as per the equation

$$Q_t = Q_0 e^{(-t/\tau)} \tag{1}$$

when the load is kept constant. After one time constant, the signal strength decreases by 37% of its initial value and the steady state value is attained after approximately five time constants according to the above equation. Without the load resistance R_{load}, the sensor would behave like a strain gauge where the signal strength remains constant for a given static load.

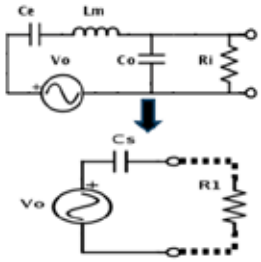

Fig. 2. Simplified electrical circuit of the sensor

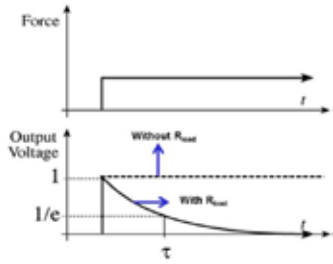

Fig. 3. Response of sensor from a static and a step input.[5]

4. SENSOR CALIBRATION

The sensor was calibrated by mounting it in a 15-
cm (6-in)-diameter steel column and by inducing sudden changes in pressure to the system. Two tests were performed; one used a ball valve and the other used a solenoid valve to calibrate the sensor at different pressure ranges and to measure the effect of the time constant on the sensitivities. The data were acquired at the rate of 1000 Hz. The sensitivity is the ratio of the signal from the sensor to the corresponding signal from the pressure transmitter at different intervals, which was found to be 50 mV/psi. The calibration curve shows that the linear calibration over a wide range of pressures, as shown in Fig. 4.

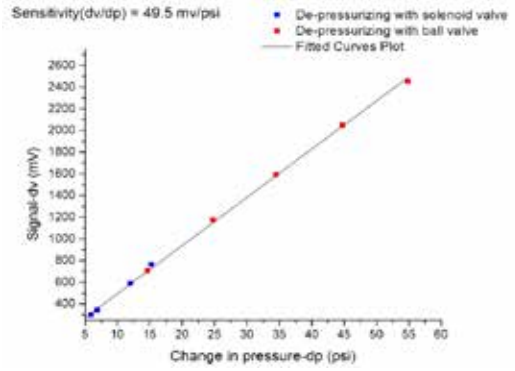

Fig. 4. Sensor calibration curve

5. EXPERIMENTAL SETUP

Two tests were performed in PSRI's 2-D fluidized bed unit using glass beads (d_{p50}=760 μm) and FCC equilibrium catalyst powder (d_{p50}=76 μm). This transparent, 2D unit provided the ability for visualization while monitoring the forces generated due to the startup of the bed and rising bubbles. Fig. 5 provides a schematic and photograph of this experimental set up. The Kistler sensor was mounted in a 0.3-m x 0.025-m (12-in X 1-in) 2D unit filled with glass beads. The bed was maintained at a minimum fluidization of 0.04 m/s (0.13 ft/s) and the corresponding bed height was 1.125 m (45 in). The injection pot pressure was at 138 kPa (20 psi) and a bubble was injected every two seconds with a solenoid valve opened for 0.5 s. The distance between the injection point and the sensor was 37.5 cm (15 in).

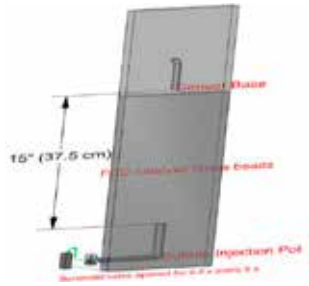

Fig. 5. Schematic of the experimental test unit used for studying the forces imparted by rising bubbles in a fluidized bed

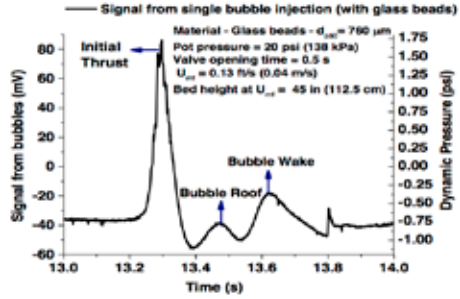

Fig. 6. Response from a single bubble injection using Geldart Group B glass beads

5.1 FORCES FROM A SINGLE BUBBLE INJECTION

The particles from both the bubble roof and the bubble wake contributed to the forces generated, with the wake being higher in force than the roof, as shown in Fig. 6. Once the solenoid valve was opened and a bubble was injected, the initial thrust caused a lot of material in the bed to lift. The total weight of the material was about 5.5 kg (12 lb). This thrust caused the initial spike in signal from the sensor, which was about 125 mV or 16.5 kPa (2.4 psi). The pressure from the wake (4.4 kPa or 0.64 psi) was much higher than the roof (2.35 kPa or 0.34 psi). In a large scale fluidized bed, these forces might actually be higher depending on the size and momentum of the rising bubbles.

5.2 FORCES DURING STARTUP OF BED

The forces induced at the startup of the bed were examined by presetting the flow rate at different gas velocities and opening the inlet gas valve when the bed was completely de-fluidized with no aeration. The valve was opened at t = 9 s and t = 12 s for the bed with FCC catalyst particles and glass beads, respectively. Fig. 7 and Fig. 8 show start up responses for both materials. The forces during the bed expansion stage depended on the material and the size of particles. For Group A powders, larger forces were observed during the bed expansion phase for the same bed height and superficial gas velocity as opposed to Group B powders. Presumably, this was due to the Group A powder's higher surface to volume ratio (and higher drag). This makes the gas less permeable and hence, more pressure builds at the bottom of the bed, which forces the gas to lift more material. Also, particulate bed expansion for Group A particles are significantly higher than that for Group B solids. Due to the initial resistance of the bed and the low permeability of the gas, there was a high dynamic pressure generated due to the bed being lifted. After the bed expands, the resistance of the bed decreased and bubbles started forming at t = 11 s for Geldart Group A FCC and t = 14 s for Geldart Group B glass beads.

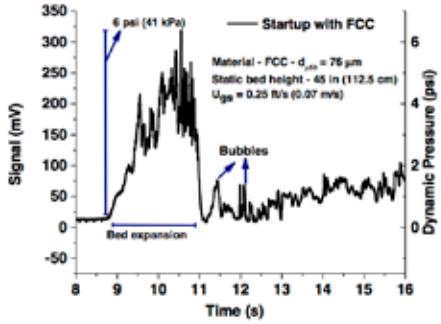

Fig. 7. Forces during startup of bed using Geldart Group A FCC catalyst with the bed fluidized at 1 ft/s (0.3 m/s) superficial gas velocity

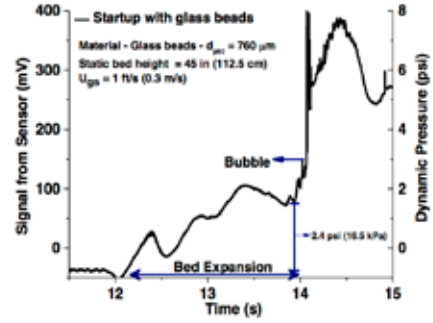

Fig. 8. Forces experienced during the startup of the bed with Geldart Group B Glass beads bed fluidized at a superficial gas velocity of 1 ft/s (0.3 m/s)

Fig. 9A and 9B show the responses from the bed expansion profile over a three-minute period during the start-up and the bubble hydrodynamics in the freely bubbling bed. The slope of the signal peaks indicated whether the forces were caused by the rising bubbles or by the expansion of the bed. The slope of the curve at startup during the bed expansion phase was much lower as opposed to the slope of the signal from the bubbles. The bed expansion was like a slow response function (low frequency response) which was reflected in the slope of the signal. The bubbles, on the other hand, reside on the sensor for a shorter time and hence the response was akin to an impulse with the slope being much higher (high frequency response). The response from the startup lasted for about three seconds, while the response from the bubbles was for about 0.07 s.

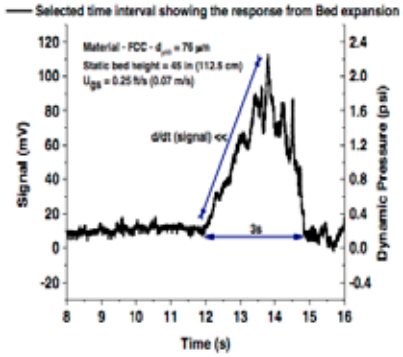

Fig. 9A. Responses from bed expansion during startup in the fluidized bed

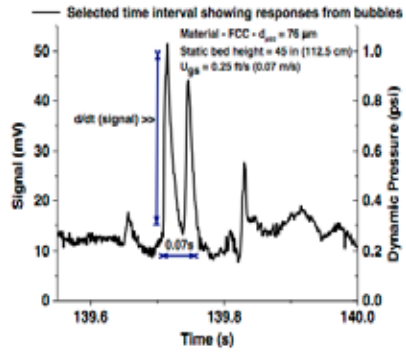

Fig. 9B. Responses from freely moving bubbles in the fluidized bed

5.3 FORCES IN A FREELY BUBBLING BED

Fig. 10A and 10B show the responses from the bed fluidized with a superficial gas velocity of 0.3 m/s (1 ft/s) using FCC catalyst particles and glass beads. The glass beads exerted larger forces (17.3 kPa or 2.5 psi) than FCC bed material (3.45 kPa or 0.5 psi) for the same superficial gas velocity and static bed height. This is primarily due to bigger bubbles for Group B solids than those for Group A solids. The responses from the bubbles in the bed of FCC material tended to have a much higher slope than for bubbles in the bed of glass beads. This suggests that the residence time on the sensor for bubbles in a Group A bed was less than for the bubbles in a Group B bed. The frequency of bubbles was also higher for FCC catalyst material in this test, as a higher number of signal peaks occurred within a certain time frame.

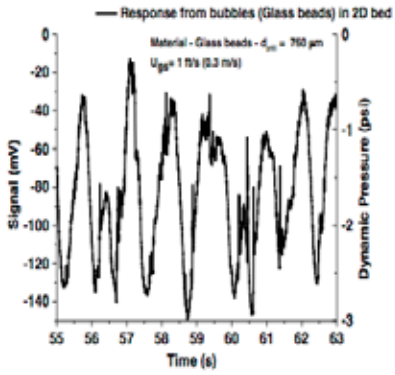

Fig. 10A. Responses from Geldart Group A FCC material in a freely bubbling bed

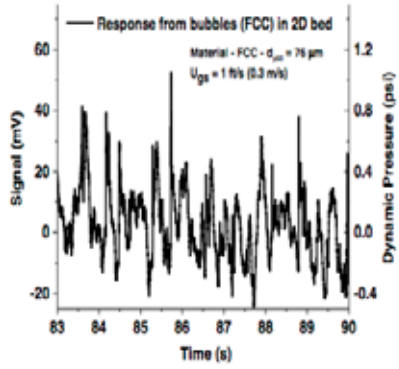

Fig. 10B. Responses from Geldart Group B glass beads in a freely bubbling bed

5.4

FORCES FROM JETS

The injection pot pressure was increased to 206.3 kPa (30 psi) and the solenoid valve opening time to 0.8 s while the other initial conditions remained similar to those in Section 5.1. The wake of the jet again was responsible for the most significant induced force, which was about 22 kPa (3.2 psi), as shown in Fig. 11.

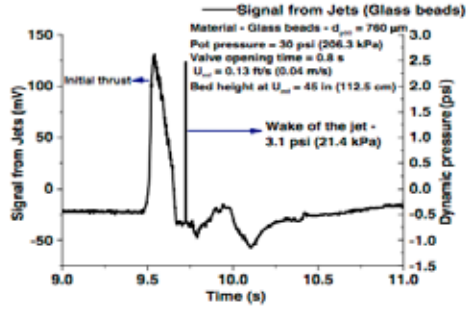

Fig. 11. Forces from jets imparted by the injection pot with Geldart Group B Glass beads

However, the thrust of the bed was almost equal to the wake. The force from gas jets were significantly higher than that found with the bubbles and suggests additional design specifications may be needed for internals in the region of gas jets.

5.5 RANDOM EVENTS THAT PRODUCED LARGER FORCES

There were two random events in a three-minute interval which induced significant dynamic forces of 110 kPa (16 psi) and 138 kPa (20 psi), as shown in Fig. 12A and 12B. When the data were plotted in real time and synchronized with the observations of the bubbling bed, it was observed that a large bubble spun clockwise and a large amount of material from the wake of the bubble might have induced this high force. Random events like these may occur over time, eventually leading to the damage of internals

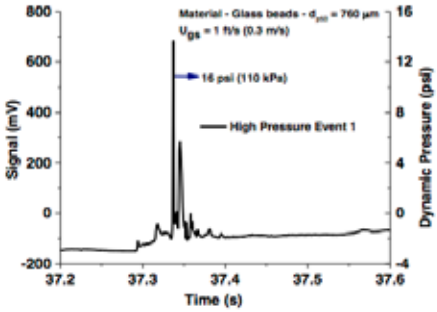

Fig. 12A. Event 1 that caused tremendous forces in the bed with Geldart Group B Glass beads

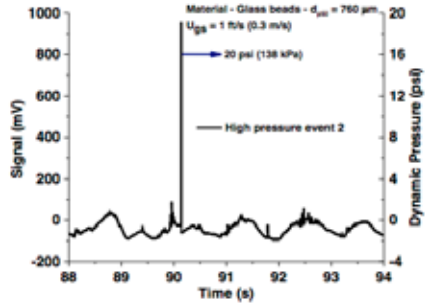

Fig. 12B. Event 2 that caused tremendous forces in the bed with Geldart Group B Glass beads

in the bed. In other words, these more intense but periodic events may have more of an impact on bed internals than a continuous exposure to a constant stream of well-behaved bubbles.

6. CONCLUSIONS

A dynamic force sensor based on the principle of piezoelectricity was used in fluid-particle systems to measure the dynamic pressures exerted by bubbles, jets, and moving particle phases on bed internals. The sensor was calibrated dynamically and the sensitivity was about 50 mV/psi (7.3 mv/kPa). The sensor was mounted in a 0.3-m x 0.03-m (12-in X 1-in) 2D, transparent unit to visually monitor the effects of fluidizing Group A and Group B powders in conjunction with the resulting signal responses. The conclusions from this study are summarized below:

- The bed was at minimum fluidization and a single bubble was injected directly below the sensor. The sensor responded to both the bubble roof and the bubble wake, with the force from the wake being higher than the roof. The bubbles generated by Geldart Group B glass beads imparted more force than that of Geldart Group A FCC catalyst particles at the same superficial gas velocity and bed height,
- FCC material exhibited greater forces during the startup of the bed due to lower permeability of the gas and higher particulate expansion of the bed material when compared to glass beads
- Dynamic force sensor data indicate that the start-up of fluidized bed needs to done in very slow fashion until the bed is fluidized. Quick start-up could generate sufficiently high dynamic forces that could damage the internals
- The forces imparted by jets were also monitored and were found to be much higher than the bubbles, and
- There were two random events which occurred in the bed that caused significantly higher dynamic forces. These events, over time, could be responsible for tube failures.

NOTATION

Q_t	Charge at time t	t	time
Q_0	Initial charge	τ	time constant
Ri	Parallel resistance	L_m	Inductance
C_e	Series capacitance	Cs	Overall capacitance
R_l	Load resistance	C_0	Parallel capacitance

7. REFERENCES

Hosny, N., and J.R. Grace, "Transient forces on tubes within an array in a fluidized bed", AIChE Journal, *30*, pp 974-976 (1984)

Karri, S. B. R., A. Issangya and T. M. Knowlton, "Gas Bypassing in Deep Fluidized Beds", in Fluidization XI, Sorento, Italy U. Arena, R. Chirone, M. Miccio and P. Salatino, eds., 515 – 521 (2004)

Inman, D. J., J. J. Dosch and E. Garcia, "A Self-Sensing Piezoelectric Actuator for Collocated Control," Journal of Intelligent Materials and Smart Structures, *3*, pp 166–18, (1992)

Lowe, O.B. and W. Resnick, "Particle and Bubble Behavior and Velocities in a Large-Particle Fluidized Bed with Immersed Obstacles," Powder Tech., *22* (1979)

Nagahashi, Y., Y. Asako, K.S. Lim, and J.R. Grace, "Dynamic forces on a horizontal tube due to passing bubbles in fluidized beds", Powder Technology, 98, pp 177-182 (1998)

Nguyen, T. H. and J. R. Grace, "Forces on Objects Immersed in Fluidized Beds," Powder Tech., *19*, 255 (1978)

http://www.intertechnology.com/Kistler/pdfs/Pressure_Model_211B.pdf, " Miniature, High Sensitivity, Voltage Output Pressure Sensors"

https://ccrma.stanford.edu/CCRMA/Courses/252/sensors/node15.html, "Signal Conditioning: Voltage to Voltage"